

Limits on the star formation rates of $z > 2$ damped Ly α systems from H α spectroscopy

Andrew J. Bunker,^{1,2} Stephen J. Warren,³ D. L. Clements,⁴
Gerard M. Williger^{5,6} and Paul C. Hewett⁷

¹University of Oxford, Department of Physics, Astrophysics, Keble Road, Oxford OX1 3RH

²Present address: University of California at Berkeley, Department of Astronomy, 601 Campbell Hall, Berkeley, CA 94720, USA

email: bunker@bigz.Berkeley.EDU

³Imperial College, Department of Physics, Blackett Laboratory, Prince Consort Road, London SW7 2BZ

⁴Department of Physics and Astronomy, University of Wales Cardiff, P.O. Box 913, Cardiff, Wales CF23YB

⁵MPIA, Königstuhl 17, D-69117 Heidelberg, Germany

⁶Present address: NASA Goddard Space Flight Center, Code 681, Greenbelt, Maryland 20771, USA

⁷Institute of Astronomy, Madingley Road, Cambridge CB3 0HA

Accepted
Received

ABSTRACT

We present the results of a long-slit K -band spectroscopic search for H α emission from eight damped Ly α absorbers (DLAs) at $z > 2$ with the goal of measuring the star-formation rates in these systems. For each system we searched for *compact* sources of H α emission within a solid angle $11 \times 2.5 \text{ arcsec}^2$ ($44 \times 10 \text{ } h^{-2} \text{ kpc}^2$, for $q_0 = 0.5$, $H_0 = 100 \text{ } h \text{ km s}^{-1} \text{ Mpc}^{-1}$). No H α emission was detected above 3σ limits in the range $(6.5-16) \times 10^{-20} \text{ W m}^{-2}$, equivalent to star formation rates of $(5.6-18) \text{ } h^{-2} \text{ M}_\odot \text{ yr}^{-1}$, for a standard IMF, assuming the lines are spectrally unresolved ($< 650 \text{ km s}^{-1}$ FWHM). We compare these results against the predictions of the models of Pei & Fall (1995) of the global history of star formation, under two different simplifying hypotheses: i.) the space density of DLAs at $z = 2.3$ is equal to the space density of spiral galaxies today (implying DLA disks were larger in the past, the ‘large-disk’ hypothesis); ii.) the sizes of DLAs at $z = 2.3$ were the same as the gas sizes of spiral galaxies today (implying DLA disks were more common in the past, the ‘hierarchical’ hypothesis). Compared to the previous most sensitive spectroscopic search our sample is twice as large, our limits are a factor greater than two deeper, and the solid angle surveyed is over three times as great. Despite this our results are not in conflict with either the large-disk hypothesis, because of the limited solid angle covered by the slit, or the hierarchical hypothesis, because of the limited sensitivity.

Key words: galaxies: formation – quasars: absorption lines – quasars: individual: PHL957; UM184; UM196; 0458–020; 0528–250; 2353+125

1 INTRODUCTION

The history of galaxies – when and how they formed, and how they have evolved – is a topic of enormous current interest. The traditional observational approach has been through deep imaging to define a flux-limited sample of galaxies. From the measurement of brightnesses and redshifts the luminosity function at different epochs can be constructed. There has been rapid progress in this field over the past three years, beginning with the measurement by Lilly et al. (1996) of the global star formation rate in galaxies out to $z = 1$, continuing with the remarkable success of Steidel

et al. (1996) in securing redshifts for dozens of galaxies at $z \approx 3$, and culminating in the plot of Madau et al. (1996) depicting for the first time a measurement of the history of global star formation in galaxies from today back to $z = 4$.

The measurement of quasar absorption lines allows an independent approach to studying the history of galaxies. The highest hydrogen column density absorbers seen in the spectra of background QSOs have $N(\text{H I}) \gtrsim 2 \times 10^{24} \text{ m}^{-2}$. These damped Ly α absorption systems (DLAs, Wolfe et al. 1986) contain most of the neutral gas in the Universe (Lanzetta, Wolfe & Turnshek 1995). From the redshift distribution of the damped systems, and the measured column

densities, the evolution in the co-moving density of neutral gas Ω_g can be measured (e.g., Lanzetta et al. 1991) provided the consequences of dust obscuration are accounted for. Then the analysis of the variation of Ω_g with redshift allows the measurement of the history of star formation in the Universe (Pei & Fall 1995).

The latter, spectroscopic, approach to the history of star formation in galaxies unfortunately tells us nothing about how galaxies are assembled, and the nature of DLAs is currently debated. One school of thought has DLAs being the (large) progenitors of massive spiral disks (e.g., Wolfe et al. 1986; Lanzetta et al. 1991). Evidence in support of this interpretation includes the measurement of line velocity profiles of low-ionization species consistent with those expected from lines of sight intercepting thick gaseous disks of circular velocity $\sim 200 \text{ km s}^{-1}$ (Prochaska & Wolfe 1997). In this case, however, it is difficult to reconcile the low metallicities of high-redshift DLAs (average metallicity 1/13 of solar at $z \approx 2.5$, Pettini et al. 1997) with the metallicities of stars in spiral disks today. The proposed cold rotationally-supported disks with these large circular speeds run counter to the predictions of cosmogonical theories currently in vogue. However Haehnelt, Steinmetz & Rauch (1998), using CDM hydrodynamic simulations, have shown that irregular (small) proto-galactic clumps can give rise to absorption profiles similar to those measured by Prochaska & Wolfe. In addition, Møller & Warren (1998) have recently shown that the impact parameters of the few detected galaxy counterparts of high-redshift DLAs are small (in the context of this debate) and that the space density of the DLAs at high-redshift is probably much higher than the space density of spiral galaxies today. In this paper we refer to these different pictures as the ‘large-disk’ and ‘hierarchical’ hypotheses.

There have been extensive searches for $\text{Ly}\alpha \lambda 121.6 \text{ nm}$ emission associated with star formation in DLAs but with limited success (e.g., Smith et al. 1989; Hunstead, Pettini & Fletcher 1990; Wolfe et al. 1992; Møller & Warren 1993; Lowenthal et al. 1995). This is generally thought to be due to resonant scattering greatly extending the path length of $\text{Ly}\alpha$ photons escaping through a cloud of neutral hydrogen so that even very small quantities of dust can extinguish the line (Charlot & Fall 1991). Because the effective extinction can be extremely large this has the consequence that non-detections do not provide any useful information on the star formation rates in the DLAs. The $\text{H}\alpha \lambda 656.3 \text{ nm}$ line, although intrinsically weaker by a factor ≈ 10 , lies at a longer wavelength where the extinction is smaller, and is not resonantly scattered. In consequence a search for $\text{H}\alpha$ emission from DLAs may be more efficient than a search for $\text{Ly}\alpha$.

In this paper, we present the results of a spectroscopic survey for $\text{H}\alpha$ emission from eight damped absorption systems at $2.0 < z < 2.6$, along the line-of-sight to six high-redshift quasars. At these redshifts $\text{H}\alpha$ appears in the K -window in the near-infrared. The results are relevant to the debate on the nature of the DLAs, for, as shown in §5, if the DLAs are the counterparts of today’s spiral galaxies the associated $\text{H}\alpha$ emission is within the reach of current instrumentation. The calculation presented there uses the analysis by Pei & Fall (1995) of the global star formation rate. The average star formation rate in each DLA depends then on their space density, so that high measured rates of star formation would provide support for the view that the DLAs

are massive galaxies already in place at high-redshift. A low measured star formation rate on the other hand would be in agreement with the hierarchical picture.

The layout for the remainder of the paper is as follows. In §2 we describe the near-infrared spectroscopic observations and in §3 the data reduction. The results are used to constrain the star formation rates in §4. The reader who is not interested in the technicalities of the survey could proceed directly to §5, where we compare these results against the predictions of the large-disk and hierarchical hypotheses. In §6 we consider the implications for strategies for detecting emission from DLAs and summarise our conclusions. Appendix A gives the results from the spectroscopy of the background quasars, and Appendix B describes the near-infrared properties of a companion galaxy to the $z = 2.31$ DLA PHL957 (Lowenthal et al. 1995). We assume a cosmology with $H_0 = 100 h \text{ km s}^{-1} \text{ Mpc}^{-1}$, $\Lambda_0 = 0$ and $q_0 = 0.5$ unless otherwise stated.

2 OBSERVATIONS

The spectra were obtained over the nights 1995 October 17 to 19 UT at the 3.8-m United Kingdom Infrared Telescope (UKIRT) with the CGS 4 instrument. Each night was partly cloudy. The journal of observations is provided in Table 1. This lists target name, target coordinates as measured off the Digitized Sky Survey, date of observation, total integration time, and slit position angle (PA) measured east of north. The redshifts of the absorbers are provided in Table 2. The detector is a 256^2 InSb array. The instrument was equipped with the 150 mm focal length ‘short’ camera, the 75 lines mm^{-1} grating, and the 2 pixel slit. In this configuration the pixel size corresponds to 1.25 arcsec in the spatial direction and the resolving power is $\frac{\lambda}{\delta\lambda} \approx 450$ (confirmed by measuring the spectral width of arc and sky lines). The seeing varied within the range 0.7–1.2 arcsec, and was therefore much less than the slit width of 2.5 arcsec.

The targets were acquired by peaking-up on a nearby bright Carlsberg Meridian Circle star, zeroing the telescope coordinates, and then moving to the QSO position. The combined accuracy associated with the acquisition and astrometry is estimated to be ~ 0.5 arcsec. With the exception of one target the central wavelength was set to $2.17 \mu\text{m}$, which placed the wavelength range $1.86 \mu\text{m} \lesssim \lambda \lesssim 2.52 \mu\text{m}$ on the array and captured the entire K -window. For one of the two PAs used in spectroscopy of PHL957 the grating angle was set to provide coverage of the wavelength interval $1.58 \mu\text{m} \lesssim \lambda \lesssim 2.24 \mu\text{m}$, which includes the lines $\text{H}\alpha$, $[\text{O III}] \lambda\lambda 495.9, 500.7 \text{ nm}$ and $\text{H}\beta 486.1 \text{ nm}$ at the redshift of the DLA ($z = 2.31$). For this target the slit was oriented to include a nearby companion galaxy at the same redshift (Lowenthal et al. 1991). The spectrum of the companion galaxy is presented in Appendix B.

The observing procedure followed was to nod along the slit between two positions 11–15 arcsec apart, keeping the source on the chip, and following the sequence $ABBAABB\dots$. At each position A or B the detector was stepped mechanically over four half-pixel increments. This enables over-sampled spectra to be obtained and eliminates gaps in the spectrum due to isolated bad pixels. At each step two 15 s integrations were co-added, and then the summed integra-

QSO	Coords (B 1950.0)	Date (UT) dd-mm-yr	Int. time /min	Slit PA /°
PHL957	01 ^h 00 ^m 33 ^s .39 +13°00'10".6	17-10-95 19-10-95	56 68	-75.9 -60.5
0458-020	04 ^h 58 ^m 41 ^s .28 -02°03'34".5	17-10-95	74	-157.9
0528-250	05 ^h 28 ^m 05 ^s .21 -25°05'44".7	18-10-95 19-10-95	32 24	-34.0 -66.5
2343+125	23 ^h 43 ^m 55 ^s .42 +12°32'19".8	17-10-95	96	-35.0
UM184	23 ^h 48 ^m 24 ^s .02 -01°08'51".3	17-10-95 18-10-95	70 56	-166.4 -13.6
UM196	23 ^h 59 ^m 16 ^s .24 -02°16'22".6	18-10-95	64	-71.4

Table 1. Journal of spectroscopic observations.

tions at the four steps were interleaved to produce a single ‘observation’ comprising 2 min of integration. The individual integration time of 15 s was set so as to avoid saturation of the strongest OH lines while ensuring that at all wavelengths the sky Poisson noise dominated the read out noise, which was approximately $15 e^-$. The dark current of CGS 4 is negligible, $< 1 e^- s^{-1}$.

3 DATA REDUCTION

The first stage in the data reduction was to divide each sub-frame by a normalised flat-field frame. The four sub-frames, stepped at half-pixel intervals, were then interleaved, with logged bad pixels ignored. This produced a frame at each nod position with 514 sample points along the dispersion axis, from the original 256 pixels. By tracing the position of arc lines across the argon arc reference frames a two-dimensional (2D) dispersion solution, rms 0.2 nm, was computed and the frames were transformed on to a linear wavelength scale, with dispersion 1.32 nm per pixel. To compensate for non-uniformities in the slit profile an illumination correction was applied, determined by collapsing the sky along the dispersion axis.

First-order sky subtraction was achieved by forming the difference image of the adjacent frames at positions *A* and *B*. The *A* - *B* pairs for each QSO and each slit PA were then summed separately using a sigma-clipping algorithm to eliminate discrepant data values, due, e.g., to cosmic rays. Residual sky counts were then removed by fitting a low-order polynomial to each column in the combined frame. The frames at this stage therefore contain a positive spectrum at position *A* and an independent negative spectrum at position *B*, so that a combination was formed by subtracting from the original a shifted version of the frame, with the two spectra registered.

The spectra were corrected for atmospheric absorption and flux calibrated using observations of A and F spectral-

type standard stars. Stellar absorption features in the spectra of the standard stars were firstly interpolated across. The standard-star spectra were then divided into a black-body curve of the appropriate temperature, scaled to the flux level corresponding to the known *K* magnitude. The resulting curves were used to calibrate the spectra. The calibration curves from night to night agreed to within 5 per cent, so the standards do not appear to have been affected by clouds. It was then possible to check the effect of clouds on the quasars by comparison of the *K*-band magnitudes measured from the calibrated spectra with the results from our own calibrated *K*-band images obtained in a complementary programme (Bunker et al. 1995; Bunker 1996). With one exception, UM196, we found good agreement. For the case of UM196 the spectroscopic magnitude was 0.8^m fainter than that measured in the image. This was assumed to be due to cloud and was therefore corrected for.

In order to search for line emission from the damped systems it was necessary to subtract accurately the flux from the background QSO. This was relatively straight-forward as the continua are smoothly-varying with wavelength and fairly flat in f_ν . In no case was there any confusion with lines from the QSO. A low-order function, usually a first-order cubic spline, was fitted to each row occupied by the QSO in the 2D spectrum around the predicted H α wavelength, excluding the region within $\sim 1000 \text{ km s}^{-1}$ of the expected line wavelength. An example of the results is shown in Fig. 1 which plots the portion of the spectrum of the QSO 2343+125 around H α , together with the continuum fit, and the continuum-subtracted spectrum. The noise was computed on the basis of Poisson statistics and is also shown in the plot. Because the quasars are $\gtrsim 20$ times fainter than the sky in *K* the contribution of the shot noise from the QSO spectrum is minimal. We also computed the standard deviation of the counts in the sky at each wavelength, up each column, as a check on the Poisson estimate of the noise, and found good agreement. The sensitivities reached (Tables 1 & 2) are similar to those quoted in the CGS 4 manual, which for a 1 pixel-wide slit (1.25 arcsec) are a 3σ detection of unresolved line emission at $2.2 \mu\text{m}$ in 30 min of $8 \times 10^{-20} \text{ W m}^{-2}$.

4 RESULTS: UPPER LIMITS ON LINE EMISSION FROM THE ABSORBERS

The choice of aperture size for extraction of the spectra depends on the expected spatial distribution of the regions of star formation in the DLAs. It should be noted that under the large-disk hypothesis the DLAs have large radii, typically $R \approx 30 h^{-1} \text{ kpc}$ at $z \approx 2.3$ for $q_0 = 0.5$, or ≈ 8 arcsec. If the H α emission is spread approximately uniformly over the disk then a large aperture matching the disk size reaches the deepest flux limit. If on the other hand most of the star formation is concentrated at one point the deepest flux limit is achieved by searching for emission lines in several parallel apertures, along the slit, each of width equal to the expected size of the region of star formation. The strategy we adopted was to use nine spatially contiguous apertures of size 1 pixel = 1.25 arcsec, one centred on the quasar, and four on either side. (The 2D long-slit spectra were also carefully inspected at larger offsets along the slit to ensure that no line emission intersected by the slit

QSO	z_{abs}	$n(\text{H I})$ 10^{24} m^{-2}	Refs.	$f_{\text{H}\alpha}$ (3 σ)	$q_0 = 0.5$		$q_0 = 0$	
				$10^{-20} \text{ W m}^{-2}$	$L_{\text{H}\alpha}$ (3 σ) $10^{34} h^{-2} \text{ W}$	SFR (3 σ) $h^{-2} \text{ M}_\odot \text{ yr}^{-1}$	$L_{\text{H}\alpha}$ (3 σ) $10^{34} h^{-2} \text{ W}$	SFR (3 σ) $h^{-2} \text{ M}_\odot \text{ yr}^{-1}$
PHL957 (both)	2.3091	25 ± 3	1, 2, 3	6.52	6.24	5.57	17.4	15.5
PHL957 (PA = -75.9°)				9.70	9.28	8.28	25.8	23.1
PHL957 (PA = -60.5°)				8.80	8.42	7.52	23.4	21.0
0458-020	2.03950	45 ± 10	1, 3, 4	9.03	6.53	5.83	16.5	14.7
0528-250 (both)	2.14030	5	5	10.0	8.09	7.23	21.2	18.9
0528-250 (PA = -34.0°)				13.3	10.7	9.57	28.1	25.1
0528-250 (PA = -66.5°)				15.3	12.4	11.0	32.4	28.9
2343+125	2.4302	3	6	7.02	7.53	6.73	21.9	19.6
UM184a (both)	2.6145	18 ± 3	3, 5, 7	10.5	13.3	11.9	41.3	36.8
UM184a (PA = -166.4°)				14.1	17.9	16.0	55.3	49.4
UM184a (PA = -13.6°)				15.8	20.0	17.8	61.9	55.2
UM184b (both)	2.4261	3.0 ± 0.5	3, 7	7.53	8.05	7.18	23.4	20.8
UM184b (PA = -166.4°)				10.1	10.8	9.64	31.3	28.0
UM184b (PA = -13.6°)				11.3	12.1	10.8	35.0	31.3
UM196a	2.1537	2.0	4	10.0	8.21	7.33	21.6	19.3
UM196b	2.0951	4.5	4	10.5	8.10	7.23	20.9	18.6

References: (1) Meyer & Roth (1990); (2) Pettini, Boksenberg & Hunstead (1990); (3) Pettini et al. (1994); (4) Wolfe et al. (1993); (5) Sargent, Steidel & Boksenberg (1989); (6) Sargent, Boksenberg & Steidel (1988); (7) Turnshek et al. (1989).

Table 2. The 3 σ upper limits for H α emission from the eight damped Lyman- α systems. This assumes the lines are unresolved ($< 650 \text{ km s}^{-1}$ FWHM), that all the star formation from the DLA is concentrated in a region smaller than $1.25 \times 2.5 \text{ arcsec}^2$, and that this region of star formation falls somewhere in the $11 \times 2.5 \text{ arcsec}^2$ solid angle searched. Where the data were taken at two different PAs, we quote the sensitivity in the region of overlap (centred on the QSO), as well as for the individual PAs.

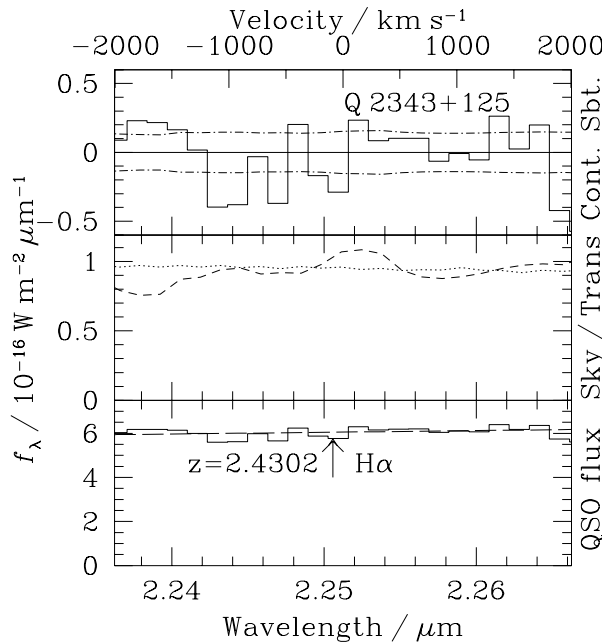


Figure 1. Example of the data showing the spectrum of the QSO 2343+125 ($z_{\text{abs}} = 2.4302$) over the velocity range 2000 km s^{-1} either side of the predicted wavelength of H α at the redshift of the damped Ly α system seen in the QSO spectrum. The bottom panel shows the QSO spectrum (solid line) with the continuum fit (long-dash line). The middle panel shows the fractional atmospheric transmission (dotted line) and the sky spectrum scaled down by a factor of 1000 (short-dash line). The top panel shows the continuum-subtracted spectrum (solid line) and the $\pm 1\sigma$ noise per pixel (dot-dash).

at greater impact parameters was overlooked.) The quoted sensitivities for the search are valid provided: i.) most of the star formation from any DLA is compact and concentrated in a solid angle smaller than $1.25 \times 2.5 \text{ arcsec}^2$, equivalent to $\approx 5.0 \times 10.0 \text{ h}^{-2} \text{ kpc}^2$, ii.) the region of star formation falls within the $11 \times 2.5 \text{ arcsec}^2$ solid angle searched. The first assumption is certainly true of one DLA, the system at $z = 2.81$ towards the quasar 0528-250 (Møller & Warren 1998), for which the half light angular radius is $r_{0.5} = 0.13 \pm 0.06 \text{ arcsec}$. The optical angular sizes of the Lyman-break galaxies (Steidel et al. 1996) are similarly small (Giavalisco et al. 1996), and this rest-UV morphology traces the star forming regions. In §5 we quantify the fraction of DLAs for which the region of star formation would fall outside the solid angle searched.

We have made a search for line emission in the extracted one-dimensional (1D) spectra (extraction width 1 pixel = 1.25 arcsec), near the expected wavelength of H α , by integrating the counts in each continuum-subtracted spectrum over 4 pixels spectrally (i.e., 5nm, just larger than the resolution of FWHM=650 km s $^{-1}$) at all wavelengths within $\pm 2000 \text{ km s}^{-1}$ of the predicted wavelength. No lines were detected at $> 3\sigma$ significance above the quasar continuum. For our $1.25 \text{ arcsec} \times 2.5 \text{ arcsec} \times 5 \text{ nm}$ aperture, the 3 σ limits lie in the range $(6.5 - 16) \times 10^{-20} \text{ W m}^{-2}$ and are recorded in Table 2. Note that the resolution of the spectra is sufficient to separate H α from the [N II] doublet so no correction to the H α flux to account for blending is necessary. A similar search was made for [O III] $\lambda 500.7 \text{ nm}$ and H β in the H -band spectrum of PHL957. No line emission was detected above the 3 σ limit of $5.3 \times 10^{-19} \text{ W m}^{-2}$.

Also recorded in Table 2 are the H α line luminosities corresponding to the line-flux limits, and the inferred limits to the star formation rates in these systems, based on

the prescription of Kennicutt (1983), where a star formation rate (SFR) of $1 \text{ M}_\odot \text{ yr}^{-1}$ generates a line luminosity in H α of $11.2 \times 10^{33} \text{ W}$. The limits to the SFRs lie in the range $(5.6 - 18) h^{-2} \text{ M}_\odot \text{ yr}^{-1}$. The conversion between H α line luminosity and SFR is uncertain and depends on the assumed initial mass function (IMF). Kennicutt adopted an IMF similar to that of Salpeter (1955). For comparison, from the models of Bruzual & Charlot (1993) a Scalo (1986) IMF with stars in the mass range $0.1 \text{ M}_\odot < M_* < 125 \text{ M}_\odot$ yields an H α line luminosity of $L(\text{H}\alpha) = 9.4 \times 10^{33} \text{ W}$ for a star formation rate of $1 \text{ M}_\odot \text{ yr}^{-1}$ (e.g., Gallego et al. 1995).

To date there have been no published successful detections of emission lines in the near-infrared from high-redshift DLAs. A detection of [OII] $\lambda 372.7 \text{ nm}$ and H β by Elston et al. (1991) from DLA 1215+333 was not confirmed in subsequent observations (J. Lowenthal, *private communication*). The only comparable limits are those of Hu et al. (1993) who observed three DLAs and recorded 3σ upper limits to the H α flux of $\approx 3 \times 10^{-19} \text{ W m}^{-2}$. The solid angle searched was either $3 \times 3 \text{ arcsec}^2$ or $3 \times 1 \text{ arcsec}^2$ (E. Hu, *private communication*). The survey presented here, therefore, is more than twice as large, reaches flux limits over twice as deep, and covers a solid angle for each DLA over three times greater.

For comparison, the characteristic star formation rate of the Lyman break population at $z \sim 3 - 4$ is $16 h^{-2} \text{ M}_\odot \text{ yr}^{-1}$ (Steidel et al. 1999) for $q_0 = 0.5$. This is determined from the rest-UV continuum around $\lambda_{\text{rest}} \approx 1500 \text{ \AA}$, assuming a Salpeter IMF and correcting for a mean extinction of $E(B - V) \approx 0.15$ using the Calzetti (1997) reddening law. Therefore, our 3σ limiting fluxes, equivalent to star formation rates of $(5.6 - 18) h^{-2} \text{ M}_\odot \text{ yr}^{-1}$ at $z \approx 2.3$, probe SFRs which are sub- L^* for the Lyman break galaxies. Indeed, our deepest flux limit is sensitive to Lyman-break-type galaxies as faint as $0.35 L^*$. However, the relationship between these Lyman break galaxies and DLAs is unclear from the few examples of $z > 2$ DLAs detected in both optical imaging and spectroscopy. The $z \approx 2.8$ DLA 0528-250 (Møller & Warren 1993; Warren & Møller 1996; Møller & Warren 1998) has a star formation rate of only $\sim 1 h^{-2} \text{ M}_\odot \text{ yr}^{-1}$ (which would fall below our H α survey limit) based on the relatively unextinguished Ly α emission with a large rest-frame equivalent width of $W_0 \approx 5 \text{ nm}$. This is quite unlike most Lyman break galaxies, which typically exhibit much higher star formation rates ($\sim 10 h^{-2} \text{ M}_\odot \text{ yr}^{-1}$) and much lower Ly α equivalent widths ($W_0 \approx 0.3 - 2$; Steidel et al. 1996). However, the $z = 3.15$ absorber towards 2231+131 is more typical of the Lyman break population, and was indeed selected as such through broad-band imaging (Steidel, Pettini & Hamilton 1995). Spectroscopy showed Ly α in emission with a rest-frame equivalent width of $W = 2.3 \text{ nm}$ (Djorgovski et al. 1996), and the rest-frame UV continuum is around L_{1500}^* for the Lyman-break galaxies, equating to star formation rates above our 3σ H α survey limit if the reddening is $E(B - V) \gtrsim 0.1$. The impact parameters in both these cases are small: 1.2 arcsec for 0528-250 ($4.3 h^{-1}$ projected); 2.3 arcsec for 2231+131 ($8.3 h^{-1}$ projected).

5 DISCUSSION: COMPARISON OF RESULTS AGAINST PREDICTIONS OF THE LARGE-DISK AND HIERARCHICAL HYPOTHESES.

In this section we compare the measured upper limits on the star formation rates in our sample against theoretical predictions. We start with the analysis by Pei & Fall (1995) of the observed rate of decline of the cosmic density of neutral gas $\Omega_g(\text{obs})$ measured from surveys for DLAs. At any redshift $\Omega_g(\text{obs})$ will be an underestimate of the true cosmic density $\Omega_g(\text{true})$ because quasars lying behind DLAs will suffer extinction, and may therefore drop out of the samples of bright quasars used to find the DLAs. Pei & Fall correct for this bias, accounting in a self-consistent manner for the increasing obscuration as the gas is consumed and polluted as star formation progresses. In this way they determine the evolution of $\Omega_g(\text{true})$, and so the SFR per unit volume:

$$\dot{\rho}(z) = -3H_0^2 \dot{\Omega}_g(\text{true}) / (8\pi G). \quad (1)$$

The analysis of Pei & Fall is global and gives no information on the SFRs in individual galaxies. We adopt their predictions for the volume-average SFR, $\dot{\rho}(z)$, and then need to make assumptions about how many DLAs there are at the redshifts of interest, and how $\dot{\rho}(z)$ is distributed between them. The methodology for the comparison is set out in the next sub-section. We adopt two different assumptions for the space density and sizes of DLAs, the ‘large-disk’ hypothesis and the ‘hierarchical’ hypothesis, explained below.

5.1 Methodology

We begin with the parametrization of the properties of spiral galaxies locally used by Lanzetta et al. (1991) in their analysis of the statistics of DLAs, i.e., we adopt a B -band galaxy luminosity function of Schechter form, with space density normalisation Φ^* , power index s , and spiral fraction f_s , a power-law (Holmberg) relation between radius and luminosity $R/R^* = (L/L^*)^t$, and a ratio between gas radius and optical (Holmberg) radius ξ , independent of luminosity. The standard values of the various parameters are $\Phi^* = 1.2 \times 10^{-2} h^3 \text{ Mpc}^{-3}$, $s = 1.25$, $f_s = 0.7$, $t = 0.4$, $R^* = 11.5 h^{-1} \text{ kpc}$, and $\xi = 1.5$ (Lanzetta et al. 1991). L^* itself is not needed in the analysis below.

At zero redshift we distribute the SFR density $\dot{\rho}(0)$ over the galaxies by assuming the SFR in an individual galaxy is proportional to the galaxy luminosity. The global star formation rate, $\dot{\rho}(z)$, predicted by Pei & Fall increases with redshift, peaking near $z = 2$. The SFRs in the DLAs will depend then on $\dot{\rho}(z)$ and on the evolution in space density of the population. Now the average incidence of DLAs per unit redshift, dn/dz , along a 1D sight-line to a quasar is proportional to the product of the space density and the gas cross section of the absorbers. Lanzetta et al. found that the incidence of DLA absorbers at $z \approx 2.5$ was considerably higher than expected, by factors of $F \approx 3.8$ for $q_0 = 0$ and $F \approx 7.1$ for $q_0 = 0.5$, on the basis of no evolution in galaxy cross section or space density. The mean redshift of our sample, $z = 2.3$, is close to that of the Lanzetta et al. sample. To use the information on the line density we consider two different hypotheses. With the ‘large-disk’ hypothesis (LD) we assume that the space density of DLAs

at high redshift is equal to the space density of spiral galaxies locally. For consistency with the line density of DLAs we suppose under this hypothesis that all DLAs in the past were larger in radius by the factor \sqrt{F} . In this case the SFR in each DLA was larger in the past by a factor $\dot{\rho}(z)/\dot{\rho}(0)$.

An alternative hypothesis is that DLAs at high redshift had the same distribution of gas sizes as spiral galaxies locally, and that the space density was greater in the past by a factor F . We call this the ‘hierarchical’ hypothesis (H). In this case there are F DLAs at high redshift for every local spiral galaxy, each of the same size as the local spiral, and the ratio of the SFR in each high-redshift DLA to the SFR in the nearby spiral is $\dot{\rho}(z)/(F\dot{\rho}(0))$. Note that this hierarchical hypothesis is merely a single specific formulation of the hierarchical picture, and is motivated only by its simplicity. It is not a generic representation of theories of hierarchical galaxy formation. The two hypotheses LD and H, and two cosmologies $q_0 = 0$ and $q_0 = 0.5$, give four models which we call LD0, LD5, H0, and H5.

With these assumptions, the distribution functions of radius and SFR at high redshift are fully specified for the four models. This allows a direct comparison against our observational results.

5.2 The mean SFR in a sample of DLAs at $\langle z \rangle = 2.3$

Samples of DLAs are selected from spectra, so the relative numbers of DLAs of different sizes are weighted by cross section. In this sub-section we compute the mean SFR in such a sample of DLAs. This provides a convenient measure to compare against our upper limits. However the calculation takes no account of the possibility that the region of star formation falls off the slit. In the next sub-section we quantify the incompleteness due to the limited solid angle covered by the slit.

The total luminosity density of spiral galaxies integrated over the Schechter function is $\mathcal{L} = f_s \Phi^* L^* \Gamma(2-s)$ where Γ denotes the gamma function. For the large-disk hypothesis the star formation rate in the DLA counterpart of a spiral galaxy of present-day luminosity $L(0)$ is given by

$$\text{SFR}(z)(\text{LD}) = \frac{L(0)\dot{\rho}(z)}{f_s \Phi^* L^*(0)\Gamma(2-s)}. \quad (2)$$

The average SFR in a sample of DLAs follows from computing the gas-cross-section weighted average present-day luminosity of a spiral galaxy, which is given by

$$\bar{L}(0) = \frac{\Gamma(2+2t-s)L^*(0)}{\Gamma(1+2t-s)}. \quad (3)$$

This gives the following relation for the expected average SFR in a sample of DLAs

$$\overline{\text{SFR}}_{\text{DLA}}(\text{LD}) = \frac{-3H_0^2 \dot{\Omega}_g(\text{true})\Gamma(2+2t-s)}{8\pi G f_s \Phi^* \Gamma(2-s)\Gamma(1+2t-s)}. \quad (4)$$

Inserting the standard values of the various parameters we obtain finally

$$\overline{\text{SFR}}_{\text{DLA}}(\text{LD}) = -1.48 \times 10^4 \dot{\Omega}_g(\text{true}) \text{ } h^{-1} \text{ M}_\odot \text{ yr}^{-1}, \quad (5)$$

where $\dot{\Omega}_g(\text{true})$ is in units of Gyr^{-1} as provided by Pei and Fall (1995).

For the hierarchical hypothesis (H) we have

$$\overline{\text{SFR}}_{\text{DLA}}(\text{H}) = \overline{\text{SFR}}_{\text{DLA}}(\text{LD})/F. \quad (6)$$

In Fig. 2 we plot as solid curves $\overline{\text{SFR}}_{\text{DLA}}(\text{LD})$ as a function of redshift for two different cosmologies. The curves of $\dot{\Omega}_g(\text{true})$ were taken from fig. 1 ($q_0 = 0.5$) and fig. 2 ($q_0 = 0$) of Pei & Fall (1995), and are for a limiting cosmic density of neutral gas at high redshift of $\Omega_{g\infty} = 4 \times 10^{-3} h^{-1}$. For the hierarchical hypothesis the average SFR is lower by a factor $F = 7.1$ for $q_0 = 0.5$ and $F = 3.8$ for $q_0 = 0$. These predictions are plotted as dashed lines in Fig. 2, and are valid only over the limited redshift range within which F was measured.

Also plotted in Fig. 2 are the upper limits to the SFR for each DLA. In the case of absorbers observed with two slit positions the limits are those for the region of overlap of the slit coverage, i.e., the region of greatest sensitivity. We see that for $q_0 = 0$ our SFR limits lie well above the predicted mean SFR level, even for the large-disk hypothesis. To reach the predicted SFRs appears to require an 8-metre class telescope. For $q_0 = 0.5$ our limits also lie above the prediction of the hierarchical hypothesis, but well below the large-disk prediction. Therefore for this case (LD5) we could expect that some of the DLAs observed would have SFRs brighter than our measured limits. Nevertheless, whether the $\text{H}\alpha$ emission would have been detected would depend on whether the region of SFR lay in the slit. Under the hypothesis LD5 the typical radius of a DLA is very large, $\sim 30 h^{-1}$ kpc. The area covered by the slit is approximately $40 \times 10 h^{-2}$ kpc 2 . This has the consequence that a high proportion of the regions of star formation will have fallen off the slit, and the proportion is highest for the disks with the largest SFRs. We quantify the incompleteness due to the finite solid angle of the slit in the next sub-section.

5.3 The effects of finite slit size on measured SFRs

Since the distributions of radius and SFR in the DLA population are fully specified under either hypothesis, we can model the effects of the finite solid angle searched. A Monte Carlo method is used. Firstly a galaxy is selected at random from the radius distribution function weighted by R^2 (to emulate the selection function from 1D quasar sight-lines). The SFR for this size is computed, as appropriate for the cosmology and the particular hypothesis, whether LD or H. In Fig. 3 the solid curves plot the cumulative distributions of SFRs computed in this manner, for the mean redshift of our sample $z = 2.3$ and a cosmology of $q_0 = 0.5$. Fig. 4 repeats this for $q_0 = 0$. Note that the H curves are simply the LD curves with the SFRs reduced by the factor F .

Next we need to establish whether the region of star formation would fall on the slit. The galaxy is placed at a random inclination angle and a random position angle. A point on the disk is selected at random, and this is the sight line to the quasar. The slit is then placed over this point. For the purposes of this calculation we assume that all the star formation is in a compact region at the centre of the DLA. If the centre of the DLA is now found to fall in the region of the slit searched (or either slit if two PAs in Table 1 were used) the SFR is recorded, otherwise the value zero. This then is the predicted SFR that would have been measured by our survey if the integration times had

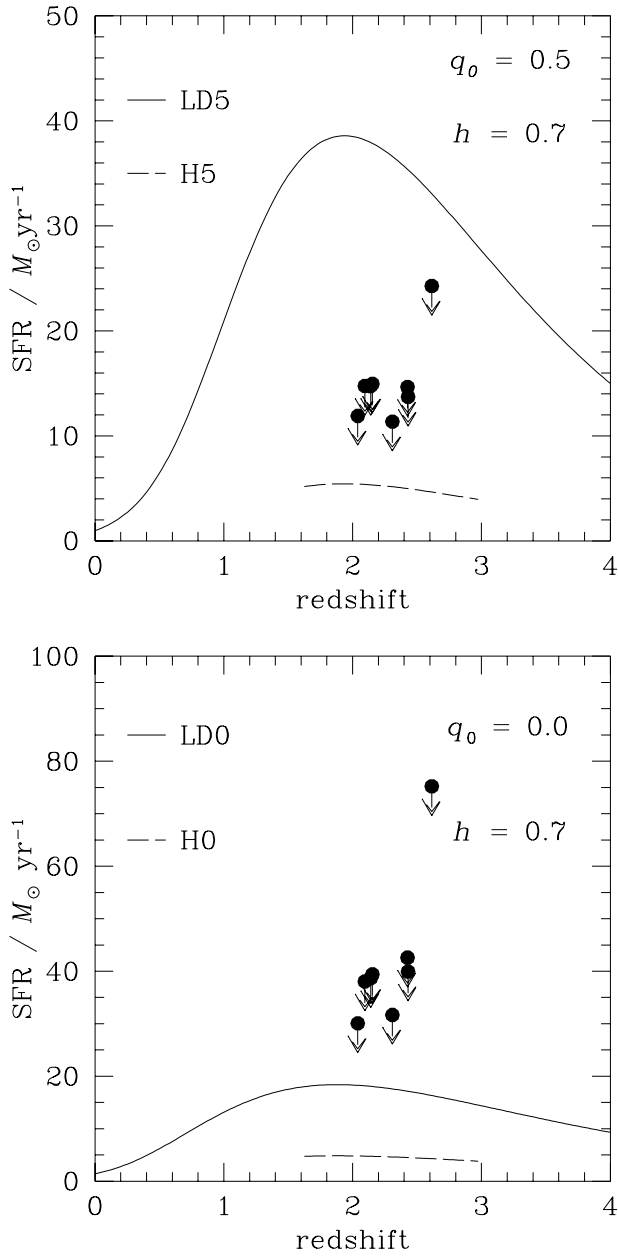


Figure 2. Comparison of observational limits to the SFRs in the sample of DLAs against theoretical predictions for $q_0 = 0.5$ (upper plot) and $q_0 = 0.0$ (lower plot). The measured 3σ upper limits for the $1.25 \text{ arcsec} \times 2.5 \text{ arcsec} \times 5\text{nm}$ extraction aperture are plotted as arrows. The solid curves are the predicted sample-averaged (i.e., cross-section weighted) SFRs for the closed-box models of Pei & Fall (1995) for $\Omega_{g\infty} = 4 \times 10^{-3} h^{-1}$, and for the large-disk hypothesis (LD). The dashed curves are the predictions under the hierarchical hypothesis (H) and are valid only over the limited redshift range shown, corresponding to the redshift range in which the parameter F was measured (Lanzetta et al. 1991). The curves plotted take no account of the possibility that the regions of star formation fall off the slit. The effect of the finite slit size is computed in §5.3.

been extremely long, sufficient to detect the faintest DLAs. This distribution is plotted as the dashed curve in each panel of Figs. 3 & 4. Each curve intersects the vertical axis at a finite value which is the fraction of DLAs that fall off the slit (for example 56 per cent in the case of LD5). Note that the dashed curves, above this start point, are skewed to lower SFRs than the solid curves. This is because it is the DLAs with large SFRs that are more likely to be missed, because larger SFRs occur in larger disks.

Finally we need to compare the depth actually reached against this ideal, to quantify how many DLAs would have been detected under each of the four hypotheses. This is achieved by comparing the SFR of each hypothetical DLA against the sensitivity as follows. For each simulated DLA if the region of star formation falls within the section of the slit searched the detection upper limit is recorded, otherwise the value zero. In the case of DLAs observed at two PAs the SFR limit corresponding to one or other slit, or to the region of overlap, is recorded, as appropriate. The stepped dot-dash line records this cumulative distribution of detection limits. Note that the dashed and stepped dot-dash lines intersect the vertical axis at the same point.

The interpretation of these results is made by comparing the dashed curve with the stepped line, for each plot. Since the stepped curve records the sensitivity of the search, and the dashed curve plots the predicted SFRs, where the stepped curve lies to the right of the dashed curve, the survey limits were not sensitive enough to detect the regions of star formation. Where the stepped curve lies to the left of the dashed curve we would have expected to see an emission line. For example for the hypothesis LD5 the two lines intersect near a cumulative probability of 0.9. This implies that we would have expected to detect H α emission from only ~ 10 per cent of our sample, or a single DLA. Our null result is only 1σ different from the LD expectation for $q_0 = 0.5$. The predicted percentage of detections for the other three plots are even smaller. The LD hypothesis is not ruled out for $q_0 = 0$, and we conclude that our survey is insufficiently sensitive to test hypothesis H for either cosmology.

6 SUMMARY AND CONCLUSIONS

To summarise, we have searched for H α emission from eight damped Ly α absorbers at $z > 2$. No H α emission was detected above 3σ limits in the range $(6.5-16) \times 10^{-20} \text{ W m}^{-2}$. We have compared our results against the predictions of the models of Pei & Fall (1995) under the ‘large-disk’ (LD) and ‘hierarchical’ (H) hypotheses. Compared to the previous most sensitive spectroscopic search, our sample is twice as large, our limits are a factor greater than two deeper, and the solid angle surveyed is over three times as great. Despite this our results are not in conflict with either hypothesis. In the case of LD this is because the solid angle searched, $2.5 \times 11 \text{ arcsec}^2$, is too small. In the case of H, although most of the regions of star formation fall in the slit (the solid and dashed curves, Figs. 3 & 4, are much closer), the sensitivity is insufficient.

The plots of Fig. 3 demonstrate in a quantitative way how inefficient spectroscopy is for testing the large-disk hypothesis. The spectroscopic searches for Ly α emission from DLAs by Pettini et al. (1995) and Lowenthal et al. (1995) are

even less efficient for this purpose, because the solid angle searched was an order of magnitude smaller than for our $\text{H}\alpha$ work. Despite reaching less sensitive flux limits narrow-band $\text{H}\alpha$ imaging searches are probably more efficient for testing the large disk hypothesis because the brightest DLA counterparts are expected to have the largest impact parameters. We will address this in a future paper where we intend to incorporate the results of the existing narrow-band searches (e.g., Bunker et al. 1995; Bunker 1996; Bechtold et al. 1998; Mannucci et al. 1998; Teplitz, Malkan & McLean 1998) into the Monte-Carlo analysis.

The measured impact parameters of the few DLAs that have been detected in imaging searches provide a further test of the large-disk hypothesis. Møller & Warren (1998) showed that the small measured impact parameters of the few confirmed or candidate counterparts of high-redshift DLAs implied that for $q_0 = 0.5$ the space density of DLAs is a factor greater than five times the space density of spiral galaxies today. This result is in conflict with LD5. If the large-disk hypothesis is eventually ruled out for a low-density cosmology as well, the plots of Figs. 3 & 4 indicate that deep spectroscopy may be the most efficient method to test the hierarchical hypothesis: because in this case the DLAs are small and will usually be covered by the slit, and because spectroscopy can reach fainter flux limits than narrow-band imaging. Flux limits a factor four deeper than those reached here would be required.

Perhaps the most promising line of attack is imaging with the HST cameras NICMOS and STIS. Here the high spatial resolution and sensitivity allow the detection of very faint sources $m_H = 23.5$ mag, $m_V = 28$ mag as close as 0.4 arcsec from the line of sight to the quasar. In this way candidate counterparts to the DLA would be identified allowing a narrower slit for the subsequent spectroscopy. By this means it would be possible to reach the required faint flux limits with an 8-metre class telescope.

APPENDIX A: NEAR-INFRARED SPECTROSCOPY OF THE QUASARS

Optimally extracted near-infrared spectra of six $z > 2$ quasars were obtained (Figure A1), enabling the continua to be measured (Table A1). Strong, broad $\text{H}\alpha$ was detected from PHL957, 0458–020, 0528–250 and 2343+125. The $[\text{O III}] \lambda 500.7$ nm line was detected in PHL957 and UM196, as well as UM184 which also exhibited broad $\text{H}\beta$. Table A2 gives the equivalent widths, fluxes, velocity widths and wavelengths for these lines. The redshifts inferred are in many instances discrepant from the literature values, which are primarily derived from rest-frame UV lines such as $\text{Ly}\alpha$, detected in the optical.

A case of particular interest is 0528–250: this sight-line intercepts a second damped absorber, a $z_{\text{QSO}} \approx z_{\text{DLA}}$ system (Møller & Warren 1993) as well as the DLA at $z_{\text{abs}} = 2.14$ which was the target of the near-infrared spectroscopy. The redshift of the second absorber is $z = 2.811$, and a puzzle has been that this is redward of the literature value for the quasar, $z = 2.77$ (Morton et al. 1980). This was determined from the high-ionization $\text{C IV} \lambda 154.9$ nm line, which is typically blue-shifted with respect to the systemic redshift. The $\text{Ly}\alpha$ emission line is unusable, being almost

completely absorbed by the damped system. From the near-infrared spectroscopy, the redshift is re-measured from the $\text{H}\alpha$ line to be $z \approx 2.806$, and the $[\text{O III}] \lambda 500.7$ nm line has a redshift of $z = 2.788$. The real QSO redshift is closer to that of the damped system than formerly thought.

In all six QSOs, the low-ionization lines $[\text{O I}] \lambda 630.0$ nm and $[\text{S II}] \lambda\lambda 671.6/673.1$ nm were undetected, with the 3σ upper limit for $[\text{O I}]$ typically $1.8 \times 10^{-19} \text{ W m}^{-2}$ if unresolved. The $[\text{S II}]$ doublet was generally too near the broad-wings of $\text{H}\alpha$ for upper limits to be placed with confidence.

APPENDIX B: THE COMPANION GALAXY TO THE PHL957 DAMPED ABSORBER

By appropriate slit orientation, a spectrum of the companion C1 ($z = 2.313$, Lowenthal et al. 1991) was obtained simultaneously with a spectrum of PHL957 (Figure B1). The large impact parameter of 48 arcsec – a projected physical distance of $190 h^{-1}$ kpc ($320 h^{-1}$ kpc) for $q_0 = 0.5$ ($q_0 = 0.0$) – argues against this being the actual galaxy responsible for the absorption in the QSO spectrum at $z = 2.309$, but rather a galaxy which is in the same group as the DLA.

The $\text{H}\alpha$ line detected by Hu et al. (1993) and Bunker et al. (1995) is confirmed at 3σ , and is spectrally unresolved ($< 650 \text{ km s}^{-1}$), centred at $2.1735 \mu\text{m}$. The inferred redshift of $z = 2.312$ agrees to within $\approx 100 \text{ km s}^{-1}$ of the measurement from $\text{Ly}\alpha$ of $z = 2.3128$ (Lowenthal et al. 1991), with the difference probably attributable to absorption of the blue wing of $\text{Ly}\alpha$. The integrated flux is $(2.3 \pm 0.8) \times 10^{-19} \text{ W m}^{-2}$, consistent with the estimates of $(3.6 \pm 1.5) \times 10^{-19} \text{ W m}^{-2}$ from Hu et al. (1993) and $(2.1 \pm 0.6) \times 10^{-19} \text{ W m}^{-2}$ from Bunker et al. (1995). The $[\text{N II}]$ doublet is undetected in our near-infrared spectroscopy. The $\text{H}\alpha$ line flux corresponds to a star formation rate of $20 \pm 7 h^{-2} \text{ M}_\odot \text{ yr}^{-1}$ ($55 \pm 19 h^{-2} \text{ M}_\odot \text{ yr}^{-1}$) using the Kennicutt (1983) relation. However, the presence of moderately strong $\text{C IV} \lambda 154.9$ nm and $\text{He II} \lambda 164.0$ nm emission, and the relatively large rest-frame equivalent width of 14 nm for $\text{Ly}\alpha$ (Lowenthal et al. 1991) argue for a significant AGN contribution.

There is a marginal (3σ) detection of unresolved $[\text{O III}] \lambda 500.7$ nm at $\lambda = 1.6589 \mu\text{m}$ with $f([\text{O III}] 500.7) = (4.3 \pm 1.5) \times 10^{-19} \text{ W m}^{-2}$, while the 495.9 nm line of this $[\text{O III}]$ doublet and $\text{H}\beta$ are undetected with a 3σ upper limit of $4.4 \times 10^{-19} \text{ W m}^{-2}$. Therefore, $f[\text{O III}] / f(\text{H}\alpha) = 2.5_{-1}^{+2}$. Although the continuum of galaxy C1 is undetected in the near-infrared spectroscopy, a marginal detection of the continuum was made in the broad-band imaging of Bunker et al. (1995). The K' magnitude is 21.0^m (2σ), so with the line contribution removed the 3σ upper-limit on the continuum flux is $f_\lambda < 1.8 \times 10^{-18} \text{ W m}^{-2} \mu\text{m}^{-1}$, $f_\nu < 3.1 \mu\text{Jy}$. This would imply the continuum luminosity density is $L_\nu(3\sigma) < 8.2 \times 10^{21} h^{-2} \text{ W Hz}^{-1}$ ($L_\nu < 22 \times 10^{21} h^{-2} \text{ W Hz}^{-1}$). The 2σ lower-limit on the rest-frame equivalent width of $\text{H}\alpha$ is 22 nm (Bunker et al. 1995).

ACKNOWLEDGMENTS

We wish to thank Tom Geballe, Gillian Wright, Thor Wold and John Davies for their help with the observations. The UKIRT is operated by the Royal Observatories on behalf

QSO	<i>K</i> -band Spec. / mag	<i>K</i> -band Imaging / mag	Interval / μm	$f_\lambda / 10^{-16}$ W $\text{m}^{-2} \mu\text{m}^{-1}$	f_ν / μJy	SNR / σ pix $^{-1}$ res $^{-1}$	$L_\nu / 10^{24}$ W Hz $^{-1}$ ($q_0 = 0.5$)	$L_\nu / 10^{24}$ W Hz $^{-1}$ ($q_0 = 0$)	
PHL957	14.70 (300 σ) 14.65 (<i>K</i>)	14.74 (300 σ) ^a	2.10 \rightarrow 2.30	5.0	800	22	42	2.91	9.22
0458-020	14.73 (650 σ) 14.78 (<i>K</i>)	14.74 (140 σ) ^b	2.22 \rightarrow 2.40	4.5	790	19	36	2.17	6.00
0528-250	15.46 (350 σ)	15.46 (200 σ) ^a	2.05 \rightarrow 2.30	2.5	400	12	23	1.53	6.72
2343+125	14.42 (500 σ)	–	2.05 \rightarrow 2.20	5.6	840	18	34	2.77	8.30
UM184	16.24 (50 σ)	16.16 (75 σ) ^c	2.07 \rightarrow 2.30	1.3	200	5.5	10	0.86	3.03
UM196	17.59 (35 σ) ^d 17.59 (<i>K</i>) ^d	16.75 (40 σ) ^c	2.05 \rightarrow 2.35	0.36	58	1.7	3.2	0.23	0.76

^a ESO 2.2-m / IRAC2B November 1993, *K'* filter^b ESO 2.2-m / IRAC2B November 1994, *K'* filter^c UKIRT / IRCAM3^d Possibly affected by cloud July 1995, *K* filter

Table A1. Measured properties of the background QSOs from the *K*-band spectroscopy. The signal-to-noise is quoted both per pixel and per resolution element ($\approx 650 \text{ km s}^{-1}$, ≈ 4 pix). The ESO 2.2-m / IRAC2B broad-band imaging uses the *K'* filter, and the flux over the same wavelength range is measured from the near-infrared spectra for comparison purposes. The magnitude from the spectra integrated over the entire *K*-window is also quoted. The only major discrepancy between the broad-band magnitudes from the imaging and the spectroscopic fluxes is for UM196.

QSO	Redshift (literature)	Wavelength / μm	Line ID	FWHM / km s^{-1}	flux f_{line} / $10^{-20} \text{ W m}^{-2}$	Luminosity $L_{\text{line}} / 10^{35} \text{ W}$ ($q_0 = 0.5$)	Redshift (measured)	EW _{rest} (nm)
PHL957	2.681	2.443 1.837	H α [O III]	5500 < 650	3400 110	455 15	1440 48	2.723 2.669
0458-020	2.286	2.1595	H α	3750	1040	97	270	2.291
0528-250	2.77	2.498 1.897	H α [O III]	2300 < 650	740 40	107 5.8	354 19	2.806 2.788
2343+125	2.515	2.344	H α	4600	4400	510	1530	2.517
UM184	3.005	$\gtrsim 1.96^\dagger$	H α	–	–	–	–	$\gtrsim 2.99$
UM196	2.817	$\gtrsim 1.906^\dagger$	[O III]	–	> 50	> 7.5	> 25	> 2.807
								> 13.2

[†] Complicated by presence of atmospheric absorption feature at $\simeq 1.98 \mu\text{m}$.

Table A2. Measured properties of the emission lines of the background QSOs in the near-infrared CGS 4 spectroscopy with UKIRT (October 1995). Tabulated are the measured wavelengths, widths and fluxes for the lines, and the corresponding line luminosity, redshift and rest-frame equivalent width (EW_{rest}) for the line identifications.

of the UK Particle Physics and Astronomy Research Council (PPARC). We thank Richard McMahon for making the co-ordinates of quasar 2343+125 available to us. We have benefited from discussions with Mike Fall, Max Pettini and Hyron Spinrad. We thank the referee, Palle Møller, for his constructive comments on the manuscript. AJB gratefully acknowledges the award of a PPARC PhD studentship while at Oxford, and subsequently a NICMOS postdoctoral fellowship at UC Berkeley.

REFERENCES

Bechtold J., Elston R., Yee H. K. C., Ellingson E., Cutri R. C., 1998, in D'Odorico S., Fontana A., Giallongo E., eds., ASP Conf. Ser. Vol. 146, The Young Universe: Galaxy Formation and Evolution at Intermediate and High Redshift, Astron. Soc. Pac., San Francisco, p. 241

A. Bruzual G., Charlot S., 1993, ApJ, 405, 538

Bunker A. J., Warren S. J., Hewett P. C., Clements D. L., 1995, MNRAS, 273, 513

Bunker A. J., 1996, D.Phil. Thesis, University of Oxford, “Searches for Distant Galaxies”, abstract in 1997, PASP, 109, 628. WWW address <http://astro.berkeley.edu/~bunker/thesis.html>

Calzetti D., 1997, AJ, 113, 162

Charlot S., Fall S. M., 1991, ApJ, 378, 471

Djorgovski S. G., Pahre M. A., Bechtold J., Elston R., Nature, 382, 234

Elston R. J., Bechtold J., Lowenthal J. D., Rieke M., 1991, ApJ, 373, L39

Gallego J., Zamorano J., Aragón-Salamanca A., Rego M., 1995, ApJ, 455, L1

Giavalisco M., Steidel C. C., Macchetto F. D., 1996, *ApJ* 470, 189
 Haehnelt M. G., Steinmetz M., Rauch M., 1998, *ApJ*, 495, 647
 Hunstead R. W., Pettini M., Fletcher A. B., 1990, *ApJ*, 356, 23
 Hu E. M., Songaila A., Cowie L. L., Hodapp K-W., 1993, *ApJ*, 419, L13
 Kennicutt R. C., 1983, *ApJ*, 272, 54
 Lanzetta K. M., Wolfe A. M., Turnshek, D. A., Lu L., McMahon R. G., Hazard C., 1991, *ApJS*, 77, 1
 Lanzetta K. M., Wolfe A. M., Turnshek D. A., 1995, *ApJ*, 440, 435
 Lilly S. J., Le Fèvre O., Hammer F., Crampton D., 1996, *ApJ*, 460, L1
 Lowenthal J. D., Hogan C. J., Green R. F., Caulet A., Woodgate B. e., Brown L., Foltz C. B., 1991, *ApJ*, 377, L73
 Lowenthal J. D., Hogan C. J., Green R. F., Woodgate B. E., Caulet A., Brown L., Bechtold J., 1995, *ApJ*, 451, 484
 Madau P., Ferguson H. C., Dickinson M. E., Giavalisco M., Steidel C. C., Fruchter A., 1996, *MNRAS*, 283, 1388
 Mannucci F., Thompson D., Beckwith S. V. W., Williger G. M., 1998, *ApJ*, 501, L11
 Meyer D. M., Roth K. C., 1990, *ApJ*, 363, 57
 Møller P., Warren S. J., 1993, *A&A*, 270, 43
 Møller P., Warren S. J., 1998, *MNRAS*, 299, 661
 Morton D. C., Chen J., Wright A. E., Peterson B. A., Jauncey D. L., 1980, *MNRAS*, 193, 399
 Pei Y. C., Fall S. M., 1995, *ApJ*, 454, 69
 Pettini M., Boksenberg A., Hunstead R. W., 1990, *ApJ*, 356, 23
 Pettini M., Smith L. J., Hunstead R. W., King D. L., 1994, *ApJ*, 426, 79
 Pettini M., Hunstead R. W., King D. L., Smith L. J., 1995, in Meylan G., ed., *ESO Astrophysics Symposia Series, QSO Absorption Lines*, Springer-Verlag, Berlin, p. 55
 Pettini M., King D. L., Smith L. J., Hunstead R. W., 1997, *ApJ*, 478, 536
 Prochaska J. X., Wolfe A. M., 1997, *ApJ*, 487, 73
 Salpeter E. E., 1955, *ApJ*, 121, 161
 Sargent W. L. W., Boksenberg A., Steidel C. C., 1988, *ApJS*, 68, 539
 Sargent W. L. W., Steidel C. C., Boksenberg A., 1989, *ApJS*, 69, 703
 Scalo J. M., 1986, *Fund. Cosmic Phys.*, 11, 1
 Smith H. E., Cohen R. D., Burns J. E., Moore D. J., Uchida B. A., 1989, *ApJ*, 347, 87
 Steidel C. C., Pettini M., Hamilton D., 1995, *AJ*, 110, 2519
 Steidel C. C., Giavalisco M., Pettini M., Dickinson M. E., Adelberger K. L., 1996, *ApJ*, 462, L17
 Steidel C. C., Adelberger K. L., Giavalisco M., Dickinson M. E., Pettini M., 1999, *ApJ, in press*
 Teplitz H. I., Malkan M. A., McLean I. S., 1998, *ApJ*, 506, 519
 Turnshek D. A., Wolfe A. M., Lanzetta K. M., Briggs F. H., Cohen R. D., Foltz C. B., Smith H. E., Wilkes B. J., 1989, *ApJ*, 344, 567
 Warren S. J., Møller P., 1996, *A&A*, 331, 25
 Wolfe A. M., Turnshek D. A., Smith H. E., Cohen R. D., 1986, *ApJS*, 61, 249
 Wolfe A. M., Turnshek D. A., Lanzetta K. M., Oke J. B., 1992, *ApJ*, 385, 151
 Wolfe A. M., Turnshek D. A., Lanzetta K. M., Lu L., 1993, *ApJ*, 404, 480

This paper has been produced using the Royal Astronomical Society/Blackwell Science \LaTeX style file.

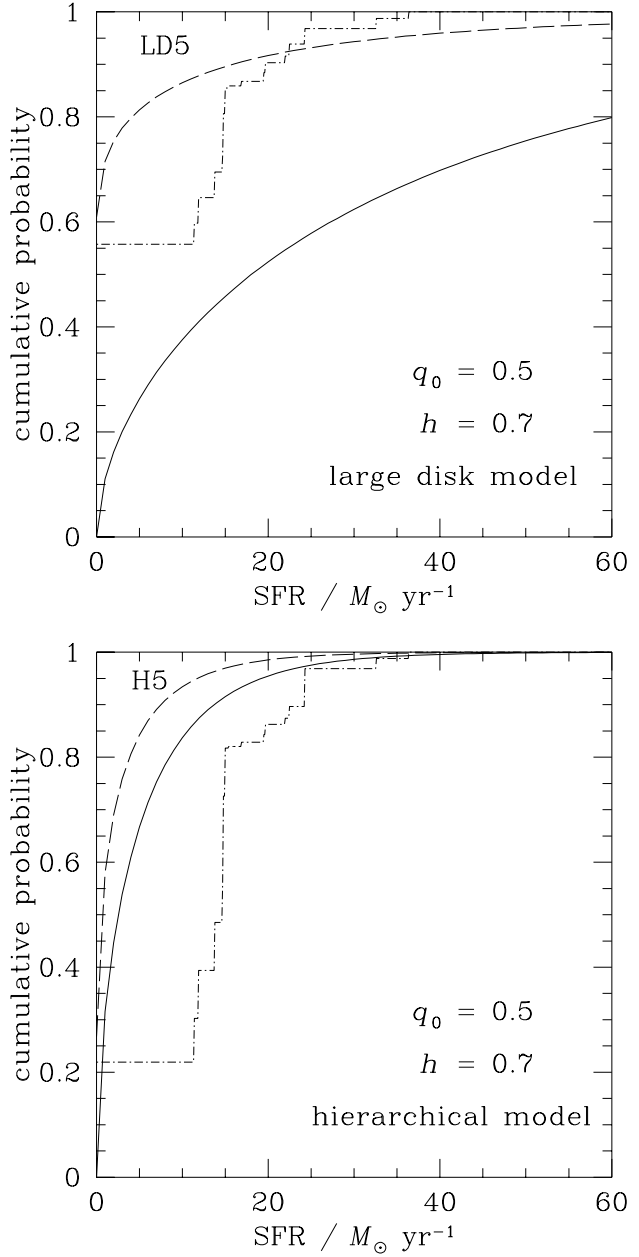


Figure 3. Predicted and observed cumulative probability distributions of SFRs for models LD5 (upper) and H5 (lower), for $h = 0.7$ and $q_0 = 0.5$. For each plot the solid line shows the predicted distribution of SFRs for a sample of DLAs at $z = 2.3$. The dashed line shows the expected observed distribution after accounting for the limited solid angle searched, 11 arcsec (spatial extent) \times 2.5 arcsec (slit width). The stepped dot-dash line plots the cumulative distribution of observational upper limits. The value of the cumulative probability at which the stepped dot-dash line crosses the dashed line is the expected proportion of DLAs that would not be detected by our survey.

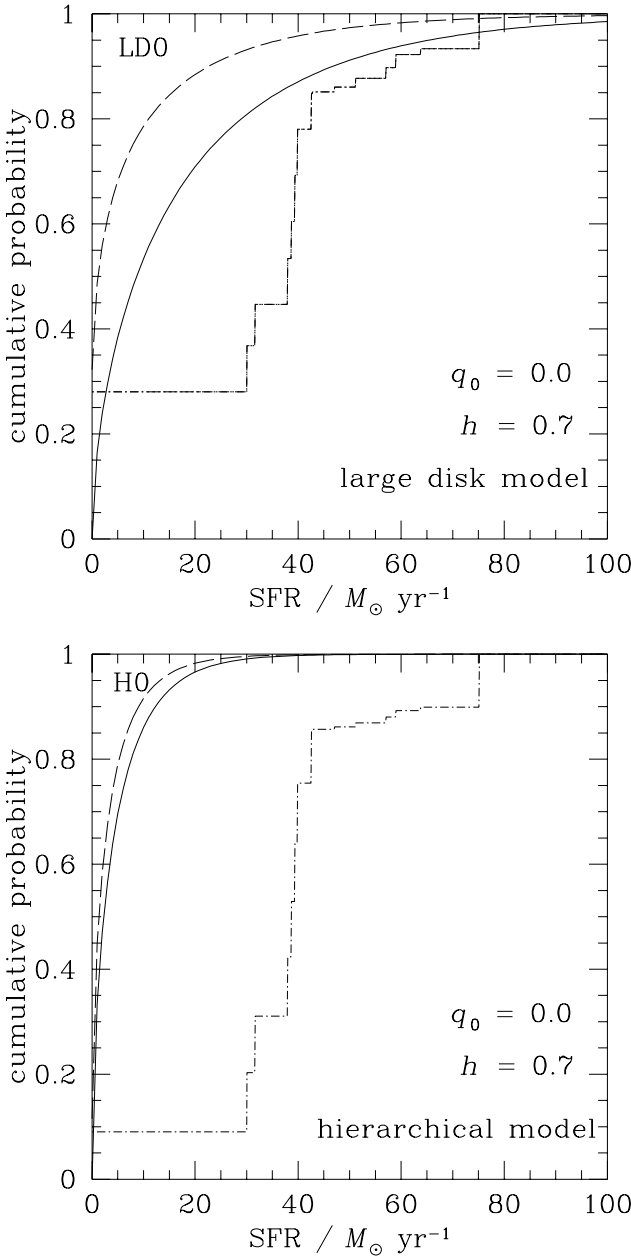


Figure 4. Predicted and observed cumulative probability distributions of SFRs for models LD0 (upper) and H0 (lower), for $h = 0.7$ and $q_0 = 0.0$. For each plot the solid line shows the predicted distribution of SFRs for a sample of DLAs at $z = 2.3$. The dashed line shows the expected observed distribution after accounting for the limited solid angle searched, 11 arcsec (spatial extent) \times 2.5 arcsec (slit width). The stepped dot-dash line plots the cumulative distribution of observational upper limits. The value of the cumulative probability at which the stepped line crosses the dashed line is the expected proportion of DLAs that would not be detected by our survey.

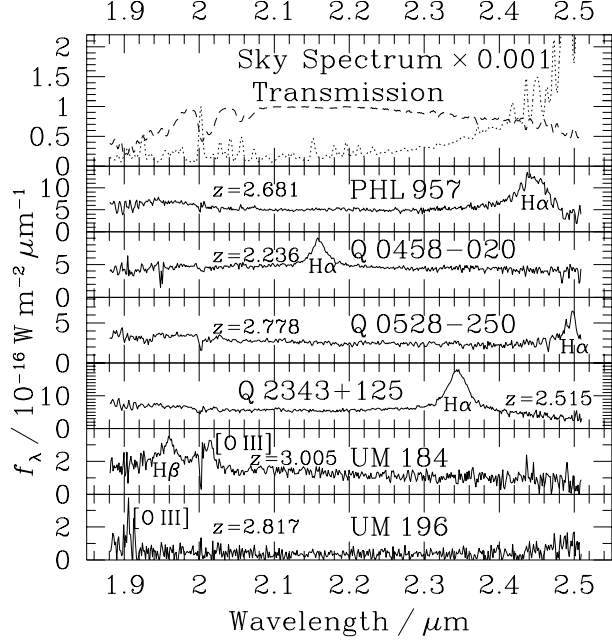


Figure A1. K -band spectra of the six target quasars, in units of f_{λ} with the prominent emission lines labelled. The top panel shows the sky spectrum (dashed line, scaled down by a factor of 1000) and the atmospheric transmission (dotted line).

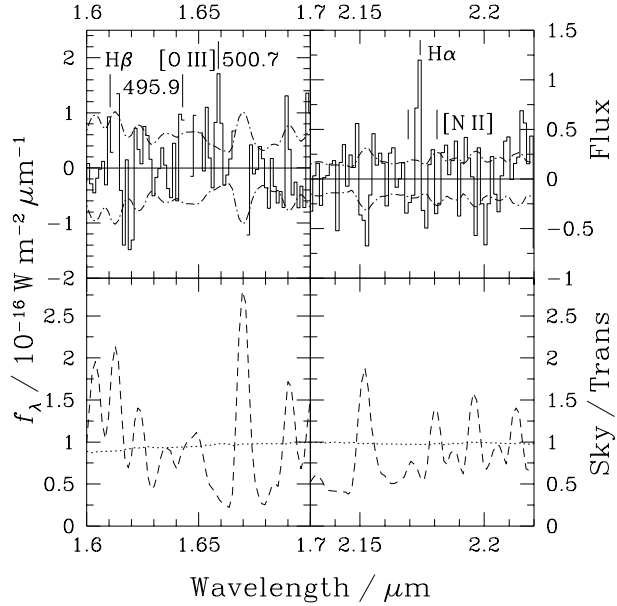


Figure B1. The H α (top-right panel) and [O III] $\lambda 500.7$ nm emission (top-left panel) from the $z = 2.31$ companion galaxy, C1, of the DLA PHL957. The dot-dash lines are the $\pm 1\sigma$ noise per pixel, and the lower panels show the fractional atmospheric transmission (dotted line) and the sky spectrum scaled down by a factor of 1000 (short-dash line).